



BOLETÍN VOL. 7, NÚM. 1
SEPTIEMBRE 2019

CONTÁCTANOS EN:



observatorio.facite@uas.edu.mx

PÁGINA WEB:



<http://facite.uas.edu.mx/>



UNIVERSIDAD AUTÓNOMA DE SINALOA
FACULTAD DE CIENCIAS DE LA TIERRA Y EL ESPACIO



Boletín Vol. 7, Núm. 1 Septiembre 2019

Contenido

ARTÍCULOS	1
GPS, Accelerometer, and Smartphone Fused Smart Sensor for SHM on Real-Scale Bridges	1
Comparative análisis of precise point positioning Processing technique with GPS low-cost in different technologies with academic software	2
Estimation of maximum mass velocity from macroseismic data: A new method and application to archeoseismological data	2
Mapping and characterization of intensity in land use by pasture using remote sensing	3
High-resolution DEM generation from spaceborne and terrestrial remote sensing data for improved volcano hazard assessment. A case study at Nevado del	4
Monitorización de la respuesta de playas mediterráneas a temporales y actuaciones antrópicas mediante imágenes Landsat	5
Photometric and astrometric study of open cluster FSR 814 (Koposov 36) using SDSS/2MASS/PPMXL/Gaia DR2	5
The AIVERSE project: Simulating, analyzing, and describing galaxies and star clusters with artificial intelligence	6
NOTICIAS	7
CONGRESOS	8
PROGRAMA DE CONFERENCIAS Y TALLERES	9

Directorio

Dr. Juan Eulogio Guerra Liera
Rector

M.C. Jesús Madueña Molina
Secretario General

Dr. Wenseslao Plata Rocha
Director

M.C. Aníbal Israel Arana Medina
Secretario Académico

Ing. Jazive Rebeca Sánchez Jacobo
Coordinadora del Observatorio Infotecnológico



ARTÍCULOS: GEODESIA, GEOMÁTICA Y ASTRONOMÍA

GPS, Accelerometer, and Smartphone Fused Smart Sensor for SHM on Real-Scale Bridges

Guzmán-Acevedo, M., Vazquez-Becerra, G., Millan-Almaraz, J., Rodriguez-Lozoya, H., Reyes-Salazar, A., Gaxiola-Camacho, J., Martinez-Felix, C., (219). *Advances in Civil Engineering*.

Abstract

During the last two decades, Global Positioning System (GPS) geodetic-grade receivers and accelerometers have been implemented in Structural Health Monitoring (SHM). Most recently, the use of sensors integrated in smartphones has been evolving. Although some of their capabilities are validated for small and local structures, there is a gap in knowledge about the use of sensors embedded in smartphones and other electronic devices for SHM of complex structures as bridges. To contribute in this area, this paper demonstrates the application of GPS receivers, accelerometers, and smartphones, integrating a smart sensor for the SHM of bridges. In order to validate its capabilities, the alternative smart sensor is used to study

a particular bridge with vibration problems. Semistatic and dynamic displacements are obtained by means of GPS measurements. Accelerations in three directions of the bridge are determined using the accelerometer and the smartphone. Based on the results of the alternative smart sensor, inappropriate structural behavior is detected in the vertical direction of the bridge. In addition, dynamic characteristics are extracted using the smart sensor applying the Fast Fourier Transformation (FFT) and periodogram to the structural responses. As a result, it is verified the applicability of the fused smart sensor for SHM on real-scale bridges.

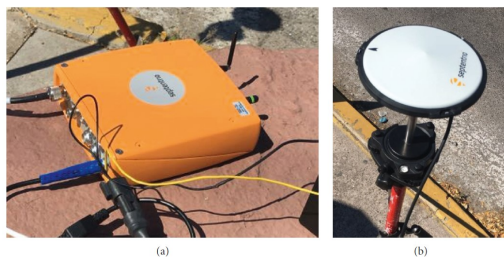


Figure 1. GPS sensors used: (a) receiver unit; (b) antenna.

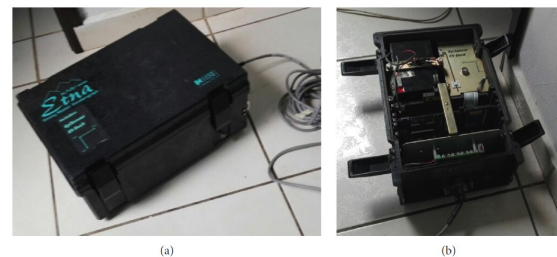


Figure 2. ETNA accelerometer: (a) outside view; (b) interior view.

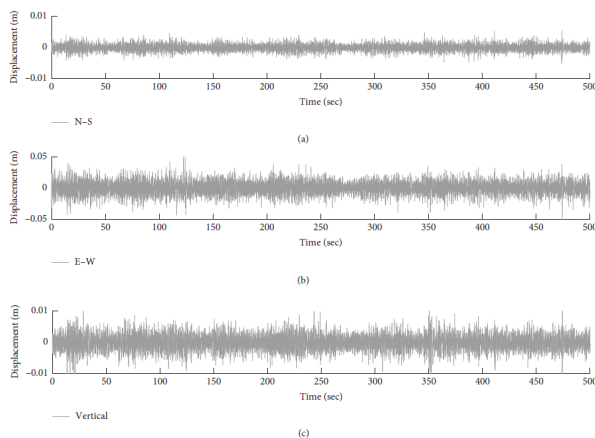


Figure 3. Dynamic displacements in three directions: (a) N-S, (b) E-W, and (c) vertical.

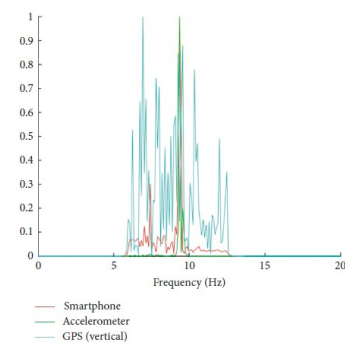


Figure 4. Dynamic frequencies in terms of periodogram (vertical direction).



Comparative analysis of precise point positioning processing technique with GPS low-cost in different technologies with academic software

Romero-Andrade, R., Zamora-Maciel, A., Uriarte-Adrián, J., Pivot, F., Trejo-Soto, M., (2019). *Measurement Journal*. Vol. 136.

Abstract

This research was conducted in order to prove the solution and accuracy that can be achieved by precise point positioning Processing technique, implementing low-cost GPS receivers with three different technologies as a Processing platform on one station situated in Culiacan, Sinaloa, Mexico. We prove the behavior and reliability of the RTKLIB software embedded system and the compares the solution with a geodetic GPS receiver by the statistical análisis. For this experiment, we use a common cellphone based in Android system, Raspberry Pi and Laptop with Linux system, all of them with RTKLIB software in a proper versión. The results showed better behavior on the embedded system; nevertheless the geodetic receiver it is more constant on the horizontal and vertical components.

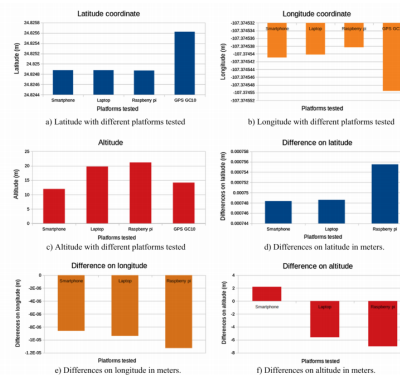


Figure 1. Positioning comparative with the platforms tested (subparagraphs a-c). Coordinates differences of each platform considering as real value the coordinates of the GC10 receiver, differenced expressed in meters.

Table 1. Results of the stimations of the CEP and VPA according to the normative of INEGI in meters.

Platform tested	σ_{ϕ}	σ_{λ}	σ	CEP ₉₅	EPV
Smartphone	0.064	0.067	0.202	0.16	0.395
Laptop	0.175	0.164	0.433	0.415	0.848
Raspberry pi	0.104	0.078	0.283	0.223	0.554
GC10	0.168	0.317	0.191	0.594	0.374

Recuperado de: <http://dx.doi.org/10.1016/j.measurement.2018.12.100>

Estimation of maximum mass velocity from macroseismic data: A new method and application to archeoseismological data

Xiang, Y., Gao, Y., Shi, J., Chaoquian, X., (2019). *Journal of Geodesy*. Vol. (93).

Abstract

Ionospheric observables based on Global Navigation Satellite System can be obtained by a variety of approaches. The most widely used one is the geometry-free combination of carrier-phase smoothed code measurements. This method, however, introduces leveling errors that substantially degrade the performance of ionospheric modeling and bias estimation. To reduce leveling errors, precise point positioning (PPP) model is preferred for obtaining the ionospheric observables. We aim to investigate whether the ionospheric observables obtained from three different PPP models are consistent and how the PPP-based ionospheric observables relates to the smoothed code method. The paper begins by formulating the ionospheric observables. We then explain the statistical evaluation methods used for analyzing the bias terms derived from these methods and assessing the leveling errors from the carrier-phase smoothed code method. Numerical analysis is then conducted to compare the bias terms in the ionospheric observables and evaluate the leveling errors. The ionospheric observables based on the three PPP models show strong consistency. Compared to leveling errors in the carrier-phase smoothed code method, the leveling errors using the uncombined PPP model are significantly reduced up to five times.

Recuperado de: <https://doi.org/10.1007/s00190-019-01233-1>

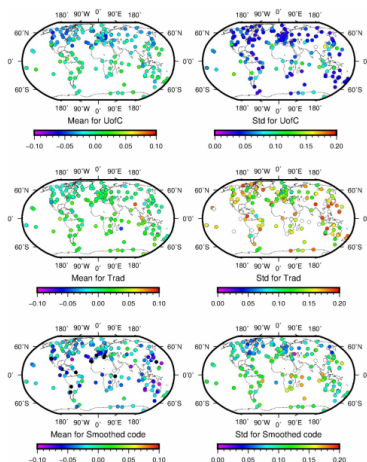


Figure 1. Geographical distribution of the station-specific mean and STD for difference of ionospheric observables from the Traditional and UofC models and the smoothed code method when compared to that from the UPPP model .



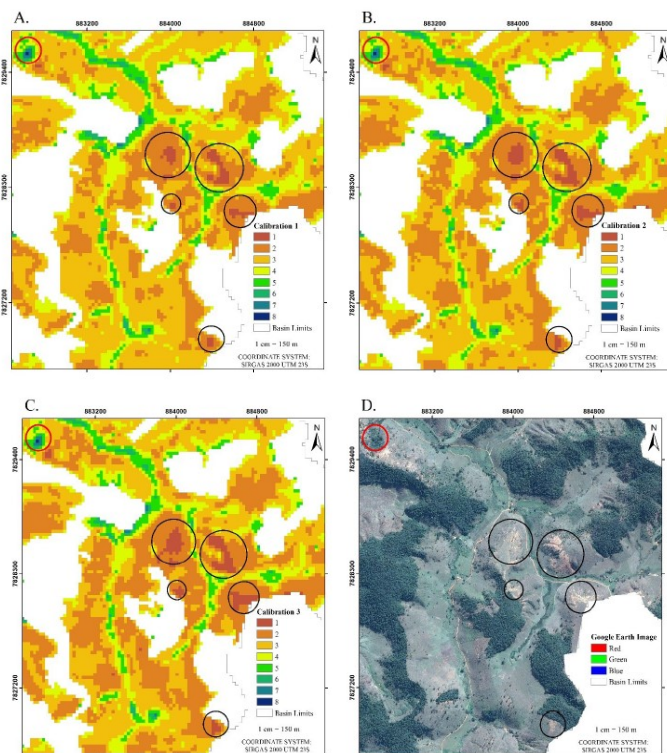
Mapping and characterization of intensity in land use by pasture using remote sensing

Calegario, A., Pereira, L., Pereira, S., Da Silva, L., De Araujo, U., Fernandes, E., (2019). *Revista Brasileira de Engenharia Agrícola e Ambiental*. Vol. 23 (5).

Abstract

The current demand for food has been met through the exploitation of natural reserves. Brazil has 26% of its extension occupied by agricultural uses, 62% of which are pastures. Degraded pastures have greater land use intensity than well-managed pastures, leading to greater degradation of the environment. Land use classification systems consider that pastures are well managed, a misconception for the Brazilian reality. Based on this approach, it was aimed to develop a methodology for mapping the intensity of land use by pasture via remote sensing. The method of mapping was developed and validated in basins with different soil and climatic characteristics. Three calibrations were performed

based on NDVI values to ascertain the influence on the results, being evaluated from the field campaigns and the kappa and weighted kappa indices. The kappa and weighted kappa indices presented reasonable and moderate agreement, respectively. The results were considered as satisfactory for the three calibrations, evidencing that the degree of degradation of the pastures can be estimated in a simple way by remote sensing. The Limoeiro River Basin has around 46.9% of pastures, at least, heavily degraded and 96.6% with some degree of degradation, which contributes to degradation of the natural resources and reduction of livestock farming and economic potential of the basin.



Basin Black and red circles indicate zones of exposed soil and forest used un the calibration, respectively.

Figure 2. Map of classification of land use intensity by pasture according to the calibrations 1 (A), 2 (B), and 3 © and Google Earht Image (D) of a portion of the Limoeiro River.

Table 1. Classes of land use intensity exerted by the pasture.

Class	Denomination
I	Exposed soil
II	Extremely degraded pastures
III	Heavily degraded pastures
IV	Moderately degraded pastures
V	Slightly degraded pastures
VI	Conservationist pastures
VII	'Capoeiras' and silvopastoral systems
VIII	Natural forests

Table 2. Percentage of áreas occupied by different classes of use intensity by pastures and values of kappa and weighted kappa for the classifications performed.

Use intensity class and Validation indices	Calibration		
	1	2	3
I	0.3	0.5	0.8
II	17.3***	22.3**	27.7**
III	50.0*	46.9*	43.3*
IV	20.1**	18.6***	17.2***
V	8.6	8.3	7.8
VI	3.0	2.9	2.7
VII	0.6	0.6	0.6
VIII	0	0	0
kappa	0.34	0.35	0.34
weighted kappa	0.62	0.66	0.62

Recuperado de: <http://dx.doi.org/10.1590/1807-1929/agriambi.v23n5p352-358>



High-resolution DEM generation from spaceborne and terrestrial remote sensing data for improved volcano hazard assessment — A case study at Nevado del Ruiz, Colombia

Fanghui Deng, Roggers, M., Xie, S., Dixon, T., Charbonnier, S., Gallant, E., López, C., Ordoñez, M., Malservisi, R., Voss, N., Richardson, J., (2019). *Remote Sensing of Environment*. Vo. 233.

Abstract

Volcanoes with rugged terrain remain a challenging target for generating high-resolution digital elevation models (DEMs), especially in tropical areas with frequent cloud cover. Using Nevado del Ruiz volcano as an example, we combined DEMs from the TanDEM-X (TDX) satellite mission, terrestrial radar interferometry (TRI), and Structure from Motion (SfM), to generate a new DEM with 10-m spatial resolution. This is the first study combining satellite radar, ground-based radar, photography, and freely available global DEMs to generate a high-resolution DEM without data gaps. TDX data from ascending and descending orbits were combined to generate the base DEM. Instead of using a raster format to fuse DEMs generated from different data sets with different resolutions, we developed a methodology based on 3-D point clouds: 1) re-georeference the 5-m TRI and ~1-m SfM DEMs to the 10-m TDX DEM using the iterative closest point (ICP) algorithm to minimize the horizontal and vertical discrepancy between DEMs; then 2) merge the multiple point clouds to generate a final DEM without data gaps using an adaptive algorithm that uses two search distances to smooth the transition at the edges of different data sets. We assess the new 10-m DEM by comparing simulated inundation zones obtained with two volcano flow models, LaharZ (for lahars) and VolcFlow (for pyroclastic flows), and find significant differences with respect to the 30-m SRTM DEM. Our LaharZ simulation over the new DEM shows a longer lahar run-out distance. For pyroclastic flows, the VolcFlow simulation over the new DEM produces highly channelized flows over the steep portions of a river channel and gives a larger extent of thicker deposits compared to those obtained with the 30-m SRTM DEM. Quantitative and qualitative geomorphic analysis suggests that up-to-date DEMs with high spatial resolution (~10m or even better) need to be generated to improve volcano Hazard assessment for active volcanoes.

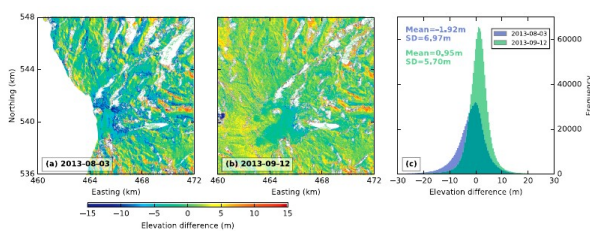


Figure 1. Elevation difference of TDX DEMs 2013-08-03 (a) and 2013-09-12 (b) relative to 2012-12-09. (c) Corresponding histograms of (a) and (b). Mean and SD are calculated and labeled.

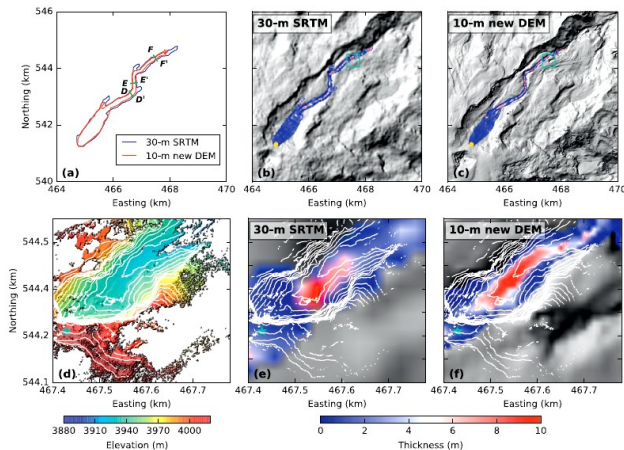


Figure 3. Simulated pyroclastic flows based on the 30-m SRTM and our new 10-m DEMs. (a) Run out of the simulated pyroclastic flows. (b) and (c) are flow thickness maps. Yellow dots indicate the starting location of the flows. Cyan boxes indicate the extent of (d), (e) and (f), which are the zoomed-in view of the waterfall area of the Azufrado channel. (d) Elevation map of the waterfall area generated from the ~1-m SfM DEM. White lines are elevation contours with an interval of 6 m. Dense contour lines indicate steep slopes. (e) and (f) are the zoomed-in view of the pyroclastic flows at the waterfall area. The head of the waterfall is indicated by cyan stars for reference. White lines are the same elevation contours as (d).

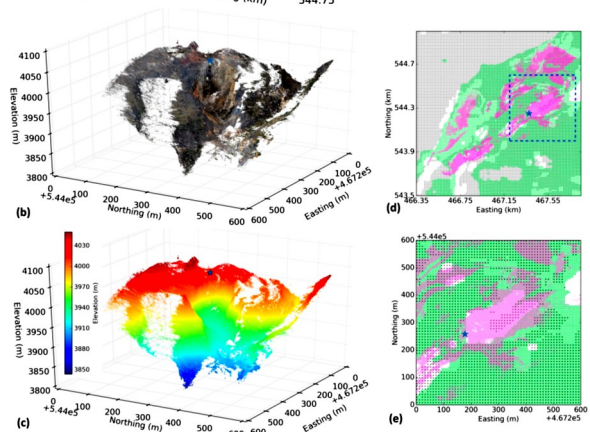
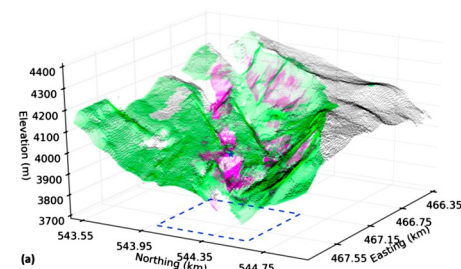


Figure 2. (a) 3D point cloud view of the TDX (black dots), TRI (green dots) and SfM (purple dots) DEMs at the upper part of the Azufrado channel. The blue box on the horizontal plane indicates the extent of (b), (c) and (e). (b) and (c) are the zoomed-in view of the SfM point cloud colored with photographic textures (Video S1) and elevation values, respectively. (d) is the 2-D view of (a). (e) is the 2-D zoomed-in view of the blue box in (a) and (d). The head of the waterfall is indicated by blue stars for reference.

Recuperado de:
<https://doi.org/10.1016/j.rse.2019.111348>



Monitorización de la respuesta de playas mediterráneas a temporales y actuaciones antrópicas mediante imágenes Landsat

Cabezas-Radabán, C., Pardo-Pascual, J., Almonacid-Caballer, J., Palomar-Vázquez, J., Fernández-Sarría-A., (2019). *Geofocus: Revista Internacional de Ciencia y Tecnología de la Información Geográfica*. Vol. 23.

Resumen

La monitorización a gran escala y de forma continua de los cambios morfológicos en playas presenta un gran interés para la gestión costera. La posición de la línea de costa ha sido definida en tres playas del golfo de Valencia en múltiples fechas durante el periodo 1984-2014 partiendo de las imágenes Landsat 5, 7 y 8 y el sistema para la extracción de líneas de costa SHOREX. Estos datos han permitido analizar la evolución de las playas durante tres décadas, así como sus cambios a corto plazo. De este modo, se ha evaluado la capacidad de las líneas para representar la respuesta de las playas ante fenómenos de temporales costeros y actuaciones antrópicas en el medio costero. Las líneas obtenidas de SHOREX muestran un gran potencial para el seguimiento y la vigilancia del estado de las playas, a la vez que el análisis de sus cambios suministra información clave de la naturaleza de las playas.

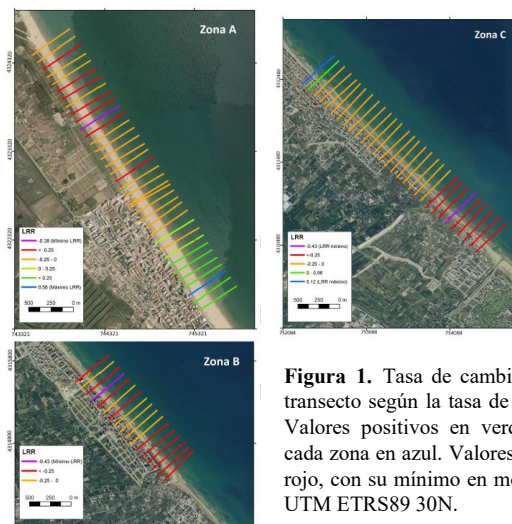


Figura 1. Tasa de cambio (1984-2014) en cada transecto según la tasa de cambio lineal (m/año): Valores positivos en verde, con el máximo de cada zona en azul. Valores negativos en naranja y rojo, con su mínimo en morado. Ortofoto PNOA, UTM ETRS89 30N.

Recuperado de: <http://dx.doi.org/10.21138/GF.640>

Photometric and astrometric study of open cluster FSR 814 (Koposov 36) using SDSS/2MASS/PPMXL/Gaia DR2

Hendy, Y.,(2018). *NRIAG Journal of Astronomy and Geophysics*. Vol. 7.

Abstract

We present multi photometric and astrometric study of open cluster FSR 814 (Koposov 36) selected from the FSRcatalog in different bands of Sloan Digital Sky Survey (SDSS), 2MASS, PPMXL and Gaia DR2. This study contains new results with a very high accuracy for the first time and generates the multi decontaminated color-magnitude diagrams to estimate the main astrophysical properties (such as: diameter, age, distance, reddening, geometrical projected distances, luminosity and mass functions) of FSR 814. Our results have been compared with other literatures.

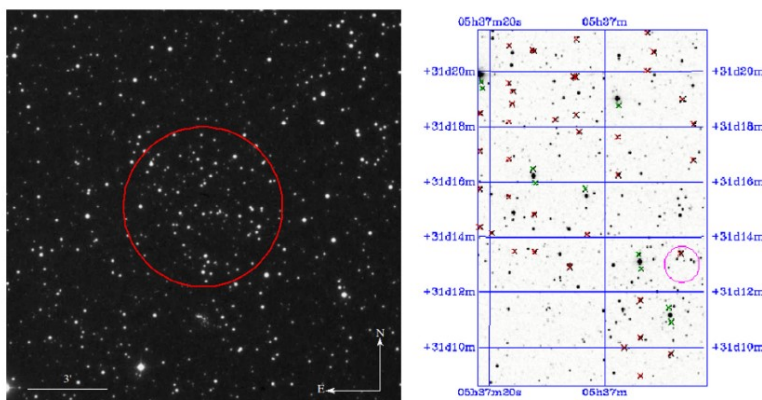


Figure 1. The left panel (R-image) and right panel (J-image) of open cluster FSR 814 are extracted from the Digitized Sky Survey (DSS) and the (Two Micron All Sky Survey) 2MASS respectively.

Recuperado de: <https://doi.org/10.1016/j.nrjag.2018.07.006>



The AVerse project: Simulating, analyzing, and describing galaxies and star clusters with artificial intelligence

Bekki, K., Díaz, J., Stanley, N., (2019). *Astronomy and Computing*. Vol. 28

Abstract

We present our new AVerse project in which several algorithm of artificial intelligence (AI) are used to simulate, analyze, and describe the physical properties of galaxies and star clusters. The three main purposes of the project are to (i) classify the formation and evolution processes of galaxies and star clusters, (ii) perform computer simulations in an automatic way, and (iii) convert the animation produced by the simulation into sentences using AI. Here we focus exclusively on the first component of the project as follows. We use convolutional neural networks (CNNs) to classify the formation and evolution processes of galaxies based on the two-dimensional (2D) images of galactic properties such as mass densities. This new classification method is two-stage as follows. First a large number of the synthesized 2D images of galactic properties from computer simulations are used to train a CNN for the classification. Once the CNN comes to have a very high accuracy, the CNN is then used to classify the real observational data. We discuss the effectiveness of the new classification method using the results of computer simulations on one of key formation processes of galaxies. We also discuss the number of images (N_i) required to generate from computer simulations by investigating the models with different N_i and other parameters. We briefly outline the other two components of the project and discuss their purposes.

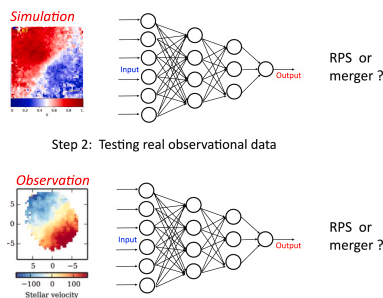


Figure 2. Illustration of the new method to convert an animation from computer simulations of galaxy formation and evolution processes into a sentence for the physical description of the processes. In the first step of this method, morphological classification of the targeted galaxy in a simulation is done for each output of the simulation using a CNN. Time evolution of the galactic morphology can be clarified in this first step. Next, classification of the formation process of the galaxy (“activity recognition”) is done by applying the LRCN method (a combination of CNNs and LSTMs e.g., (Donahue et al., 2017) to 10–20 images from the animation at selected time steps in the second step. A key physical process in the animation can be identified in this second step. The new “CER net” (cause–effect-relationship network) tries to relate the morphological evolution revealed in the first step to the formation process revealed in the second step in order to produce a sentence that describe how the formation/evolution process causes the morphological evolution.

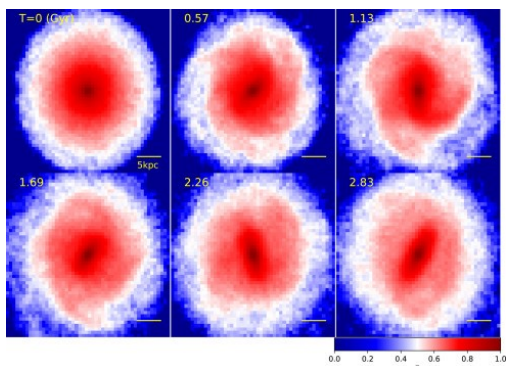


Figure 1. Illustration of the two-stage classification method based on CNNs. In the first stage, a large number of synthesized images of galaxies from computer simulations of galaxy formation and evolution are used to train CNNs. In this stage, each image is given a “label” of a particular physical process related to galaxy formation and evolution. In this figure, the 2D maps of stellar kinematics of S0 galaxies are classified into two categories, those of S0s formed from ram pressure stripping (RPS) or those of S0s from galaxy merging. Once the accuracy rate to classify between RPS and merging reaches more than a threshold value (e.g., ~95%) through the training, then we go for the second stage. The trained CNNs are used to classify the real observational data sets in this second stage. We consider the observational issues such as spatial resolution (e.g., pixel size etc.) in training the CNNs. This paper describes only the first stage of this new classification model in detail.

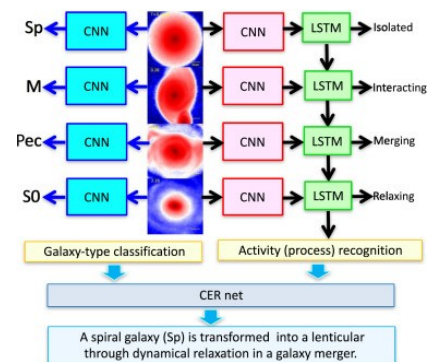


Figure 3. Time evolution of the surface mass density (Σ in logarithmic scale) of stars in a disk galaxy projected onto the x - y plane for a RPS model with $\theta=30$ degrees, $\phi=0$ degrees, $f_{v_{rps}}=0.5$, and $R_r=0.5R_{vir}$. The scale bar of 5 kpc is shown in the lower right at each panel. The mass density at each frame is normalized using all pixel values in each image (produced at each time step) so that the minimum and maximum density can be 0 and 1, respectively. This normalization is essentially important when these 2D images are fed into a CNN. Time (T) that has elapsed since the start of this simulation is shown in the upper left corner of each frame. 50×50 meshes are used to produce these images for a larger scale.

Recuperado de: <https://doi.org/10.1016/j.nrjag.2018.07.006>



NOTICIAS

La pérdida del “permafrost” y la absorción terrestre de la radiación solar en el ártico acelerarán el calentamiento

Un equipo liderado por investigadores del Consejo Superior de Investigaciones Científicas (CSIC) (España) ha evidenciado que el carbono emitido a la atmósfera por la pérdida del permafrost (la capa permanentemente congelada del subsuelo de las regiones muy frías o periglaciares) en el Ártico, junto con el incremento de la absorción de la radiación solar por la superficie terrestre, acelerarán el calentamiento global.

Las conclusiones de este trabajo, que aparece publicado en la revista Nature Communications, señalan que una

combinación de estos factores aumentará a largo plazo los costes económicos en cerca de 70 billones de dólares, un 5% del coste total estimado. Los investigadores han explorado simulaciones de modelos físicos complejos para cuantificar, por un lado, el carbono que vuelve a la atmósfera como consecuencia del derretimiento del permafrost, y, por otro, la energía solar extra que es absorbida por la superficie terrestre mientras se reduce el hielo marino y la cobertura de nieve, lo que provoca océanos y tierra más oscuros.



Noticia completa en: <https://noticiasdelaciencia.com/art/33998/la-perdida-del-permafrost-y-la-absorcion-terrestre-de-la-radiacion-solar-en-el-artico-aceleraran-el-calentamiento>

Lanzado el satélite Zhongxing-18



China lanzó el 19 de agosto un satélite de comunicaciones llamado Zhongxing-18. Sin embargo, no está claro si el vehículo está funcionando correctamente. El despegue, desde la base de Xichang, se hizo a las 12:03 UTC gracias a un cohete CZ-3B/G2 (Y58). El lanzador actuó aparentemente de forma correcta, pero las autoridades no anunciaron de forma inmediata la separación del satélite, denominado también Chinasat-18, ni su funciona-

miento conforme a lo previsto, lo que hace sospechar la existencia de algún tipo de anomalía.

La carga fue situada en una órbita de transferencia geoestacionaria. Se trata de un satélite de 5.200 kg de peso basado en una plataforma DFH-4E equipada con 30 repetidores en banda Ku y 16 en banda Ka. Debía usarse para transmitir canales de televisión, telefonía, radio e internet.

Noticia completa en: <https://noticiasdelaciencia.com/art/34004/lanzado-el-satelite-zhongxing-18>

Astrofísico gaditano realiza un nuevo descubrimiento sobre cómo se forman las estrellas

Un equipo internacional de astrofísicos de 7 instituciones en 6 países, liderado por el investigador gaditano (España) del Dublin Institute for Advanced Studies (DIAS), Rubén Fedriani, ha medido por primera vez la masa y la energía total de un chorro protoestelar lanzado por una estrella joven masiva.

Los chorros protoestelares, es decir, el material que expulsa una protoestrella (estrella joven), juegan un papel fundamental en la formación estelar. Los resultados de este estudio sugieren la existencia de un mecanismo común en la forma-

ción de chorros en protoestrellas de baja y alta masa, un nuevo descubrimiento en la formación de estrellas masivas.

El gaditano, licenciado en Matemáticas en la Universidad de Cádiz y con un Máster en Astrofísica en la Universidad Complutense de Madrid, ha estado al frente de la colaboración internacional que ha desarrollado este estudio. “Estamos un paso más cerca de afirmar que la formación de estrellas de alta y baja masa no son tan diferentes, después de todo...”.



Noticia completa en: <https://noticiasdelaciencia.com/art/33988/astrofisico-gaditano-realiza-un-nuevo-descubrimiento-sobre-como-se-forman-las-estrellas>



UNIVERSIDAD AUTÓNOMA DE SINALOA
FACULTAD DE CIENCIAS DE LA TIERRA Y EL ESPACIO



CONGRESOS



XXIII Congreso Nacional SELPER México

Sede: Centro Universitario de la Costa Sur (CUCSUR), Autlán, Jalisco

Sitio web del congreso: <https://sites.google.com/academicos.udg.mx/selper-autlan2019>



International Conference on Geospatial Information Sciences

Sede: CentroGeo, Laboratorio de Geointeligencia Nacional, Mérida, Yucatán

Sitio web del congreso: <http://igisc.org/>



RAUGM 2019 GEOCIENCIA Y SOCIEDAD

Reunión Anual de la Unión Geofísica Mexicana 2019

Sede: hotel Sheraton Baganvillas en Puerto Vallarta, Jalisco

Sitio web del congreso: <https://raugm.org.mx/>



UNIVERSIDAD AUTÓNOMA DE SINALOA
FACULTAD DE CIENCIAS DE LA TIERRA Y EL ESPACIO



PROGRAMA DE CONFERENCIAS Y TALLERES DE FORMACIÓN MULTIDISCIPLINARIA

Conferencia/Taller	Imparte	Lugar y fecha
Cómo hacer un CV	DGVRI	Aula 4 Jueves 5 de septiembre 8:30 h – 9:30 h.
Conferencia: “Historia y Geología del Yacimiento Peñasquito, Mazapil, Zacatecas”	Ing. Claudio Patricio Flores Rivera	Auditorio Viernes 6 de septiembre 16:00 h – 20:00 h.
Conferencia: “El Caos y la Complejidad en los depósitos minerales. En busca de una aproximación abstracta de la realidad”	Ing. José Antonio Martínez Mendoza	Auditorio Viernes 6 de septiembre 16:00 h – 20:00 h.
Taller: Primeros auxilios	Protección civil	Aula 6 Miércoles 11 de septiembre 16:00 h – 17:00 h.
Taller: Primeros auxilios	Protección civil	Aula 5 Jueves 12 de septiembre 8:30 h – 9:30 h.
Cómo hacer un CV	DGVRI	Aula 3 Jueves 12 de septiembre 16:30 h – 17:30 h.
Conferencia: Industrialización en la región centro de México 1989-2014	Ing. Jesús Armando Corrales Barraza	Auditorio Viernes 13 de septiembre 11:00 h – 12:00 h.
Taller: Formación de equipos de trabajo	DGVRI	Aula 7 Jueves 19 de septiembre 10:00 h – 11:15 h.

SE OTORGARÁ 1 CRÉDITO POR CADA 3 EVENTOS.



Conferencia/Taller	Imparte	Lugar y fecha
Taller: Empleabilidad	DGVRI	Aula 4 Viernes 20 de septiembre 8:00 h – 9:30 h.
Taller: Valores Universitarios	BIENESTAR UNIVERSITARIO	Auditorio Lunes 23 de septiembre 13:00 h – 14:00 h.
Taller: Formación de equipos de trabajo	DGVRI	Aula 1 Martes 24 de septiembre 14:20 h – 15:30 h.
Taller: Sitio INEGI y descarga de cartas topográficas	INEGI	Centro de cómputo Miércoles 25 de septiembre 10:00 h – 11:20 h.
Taller: Buscadores de empleo	DGVRI	Aula 3 Lunes 30 de septiembre 17:30 h – 18:30 h.
Taller: Valores Universitarios	BIENESTAR UNIVERSITARIO	Aula 7 Martes 01 de octubre 8:30 h – 9:30 h.
Taller: Batimetría (Teoría)	Ing. Iván Escalante Mondaca	Aula 4 Martes 01 de octubre 10:00 h – 13:00 h.
Taller: Batimetría (Práctica)	Ing. Iván Escalante Mondaca	Visita Jueves 03 de octubre 8:00 h.

SE OTORGARÁ 1 CRÉDITO POR CADA 3 EVENTOS.



Conferencia/Taller	Imparte	Lugar y fecha
1era. Sesión Seminario – “Proceso de Incubación”	DGVRI	Auditorio Jueves 03 de octubre 12:40 h – 15:40 h.
Taller: Valores Universitarios	BIENESTAR UNIVERSITARIO	Auditorio Viernes 04 de octubre 13:00 h– 14:00 h.
Taller: Batimetría (Procesamiento de datos)	Ing. Iván Escalante Mondaca	Centro de cómputo Lunes 7 de octubre 10:00 h – 13:00 h.
Conferencia	Dra. Xóchitl Torres Carrillo	Auditorio Martes 8 de Octubre 10:00 h – 11:00 h.
Conferencia: Espacios 100% libres de humo del tabaco	DGVRI	Auditorio Martes 15 de octubre 13:00 h – 14:00 h.
Taller ejecutivo Mapa Digital de México para escritorio versión 6.1.	INEGI	Centro de cómputo Miércoles 16 de octubre 10:00 h – 12:00 h.
2da. Sesión Seminario: “Proceso de incubación”	DGVRI	Auditorio Jueves 17 de octubre 12:40 h – 15:40 h.
Taller ejecutivo Mapa Digital de México para escritorio versión 6.1.	INEGI	Centro de cómputo Viernes 18 de octubre 12:20 h – 14:20 h.

SE OTORGARÁ 1 CRÉDITO POR CADA 3 EVENTOS.



Conferencia/Taller	Imparte	Lugar y fecha
Taller: “Computación Gráfica y Científica con Python”	Dr. Christopher Añorve Solano	Centro de cómputo Martes 22 y jueves 24 de octubre 11:00 h – 14:00 h.
Taller: “ Fotogrametría con Drones”	Dr. Juan Martín Aguilar Villegas	Centro de cómputo Lunes 28 y Martes 29 de octubre 11:00 h – 14:00 h.
3era. Sesión Seminario - “Proceso de incubación”	DGVRI	Auditorio Jueves 31 de octubre 12:40 h – 15:40 h.
Conferencia	Ing. Carlos Ramón Moraila Valenzuela	Auditorio Lunes 4 de noviembre 10:00 h – 11:20 h.
Taller ejecutivo Mapa Digital de México para escritorio versión 6.1.	INEGI	Centro de cómputo Martes 05 de noviembre 11:00 h – 13:00 h.
Taller: Valores Universitarios	BIENESTAR UNIVERSITARIO	Aula 5 Miércoles 6 de noviembre 11:30h– 12:30 h.
Taller ejecutivo Mapa Digital de México para escritorio versión 6.1.	INEGI	Centro de cómputo Jueves 7 de noviembre 10:00 h – 12:00 h.
Actividad: Desarrollo Sostenible (Visita a la reserva)	M.C. Edgar Benjamín López Camacho	Reserva Viernes 08 de Noviembre

SE OTORGARÁ 1 CRÉDITO POR CADA 3 EVENTOS.



Conferencia/Taller	Imparte	Lugar y fecha
Taller: “Uso y Manejo de Telescopios”	C. Sebastián Carrasco Gaxiola	Auditorio Lunes 11 de noviembre 17:20 h – 18:40 h.
Taller: Valores Universitarios	BIENESTAR UNIVERSITARIO	Aula 6 Miércoles 13 de noviembre 13:00 h – 14:00 h.
Curso-Taller: “Desarrollo de Interfaces gráficas con Python 3”	L.I. Jesús Abel Cota Dimas	Centro de cómputo Martes 19 de noviembre 10:00 h – 13:00 h.
Conferencia: “Competencias que demanda el mundo laboral”	DGVRI	Aula 4 Viernes 22 de noviembre 8:00 h – 9:30 h
Conferencia: “Recomendaciones para una buena entrevista profesional”	DGVRI	Aula 3 Lunes 25 de noviembre 17:30 h – 18:30 h.
Taller: Mediciones GPS	Dr. Rosendo Romero Andrade	Martes 26 de noviembre 11:00 h – 13:00 h.
Conferencia: “Gases de efecto invernadero: Cambio Climático”	Dr. Sergio Monjardín Armenta	Auditorio Miércoles 27 de noviembre 13:00 h – 14:00 h
Taller: Análisis de información obtenidas de las Mediciones GPS	Dr. Rosendo Romero Andrade	Jueves 28 de noviembre 11:00 h – 13:00 h.

SE OTORGARÁ 1 CRÉDITO POR CADA 3 EVENTOS.